Available online at www.sciencedirect.com
SCIENCE DIRECT®
Journal of Solid State Chemistry 177 (2004) 2223–2230
JOURNAL OF SOLID STATE CHEMISTRY
http://elsevier.com/locate/jssc

Observation on meta-stability of thulium nitrate crystal by using electric measurements

Riki Kawashima,* Takashi Okubo, and Hiroshi Isoda

Department of Materials Science and Engineering, Muroran Institute of Technology, 27-1 Mizomoto-cho, Muroran 050-8585, Japan

Received 22 October 2003; received in revised form 27 January 2004; accepted 7 February 2004

Abstract

Frequency dependence of ac conductivity from 1 to 10^5 Hz and time series of the conductivity at 2 kHz were measured along *c*-axis of thulium nitrate crystal, $Tm(NO_3)_36H_2O$ at temperatures from 203.15 to 293.15 K. The meta-stability was observed. The frequency spectra of the conductivity were similar to those in disorder system. Aging effect was observed. Non-periodic instability (burst) was found. Non-linear dynamical property was characterized by $1/f$ noise spectrum, limit cycle in return map and dependence of correlation exponent on embedding dimension.

Keywords: Thulium nitrate crystal; Ac conductivity; Time series data; Non-linear dynamical property

1. Introduction

Meta-stable phenomena in non-crystalline materials such as glass are amorphous and have been studied by many authors [1]. Chaotic phenomena were discovered in many non-linear systems such as chemical oscillations [2], hydrodynamics [3], and magnetic responses in ferromagnetic materials [4]. However, there has been only a small amount of information about chaotic behaviors associated to the meta-stabilities in pure crystalline one.

The rare-earth nitrate crystals $R(NO_3)_36H_2O$ where R is rare-earth element, are triclinic symmetry with the space group $P\bar{1}$, and the crystal symmetry independent of temperature above 193 K [5]. We have measured successively the electric properties between 203.15 K and room temperature in rare-earth nitrate crystals, and found meta-stable phenomena having non-ergodic non-linear property [6].

By the measurements of time series for the ac conductivity at 2 kHz, non-linear dynamical property having deterministic chaotic one were found in the rare-earth nitrate [7]. The distinct intermittent non-periodic oscillations (bursts) were observed [8]. The dependence of the rare-earth element on the time series of the ac conductivity was found in the rare-earth nitrate crystals [9].

However, the meta-stability in the rare-earth nitrate crystal was not known sufficiently. In the present paper, to clarify the characteristic phenomena, we have measured frequency spectra of the ac conductivity in the frequency region, $1\,\mathrm{Hz} \leqslant \nu \leqslant 10^5\,\mathrm{Hz}$, for several samples having different ageing periods, and the time series of the conductivity at 2 kHz, at temperatures $203.15\,\mathrm{K} \leqslant T \leqslant 293.15\,\mathrm{K}$ along *c*-axis of $Tm(NO_3)_36H_2O$ crystal. The results have been given and discussed.

2. Experimental

The crystal used for the present measurements was grown in a thulium nitrate aqueous solution by decreasing. To observe the aging effect on the electric property of the crystal, three specimens, A_1, A_2 and A_3, were prepared from the same mother crystal at different aging period. The effect was measured for the sample A_1 in the time range from 93 to 1546, for A_2 in the range from 2409 to 2766 and for A_3 in the range from 3879 to 5003 of the aging periods (hours) from the crystal growth, respectively.

*Corresponding author. Fax: +81-143-46-5601.
E-mail address: kawasima@mmm.muroran-it.ac.jp (R. Kawashima).

0022-4596/$ - see front matter © 2004 Published by Elsevier Inc.
doi:10.1016/j.jssc.2004.02.015

The dimensions of the samples A_1, A_2 and A_3 used for the measurements of the frequency spectra for the ac conductivity and those of the sample B used for measuring the time series of the conductivity were given in Table 1, respectively. The contact electrodes used in the measurements were made with silver paste (Tokuriki Chem.Inst.P255). The good qualities of the electrodes and the specimens have been kept at the final stage of the experiment [16].

The ac conductivity spectra in the frequency region from 1 Hz to 100 kHz were measured by using a computer-controlled auto-phase digital lock amplifier (EG&G Princeton Applied Research, Model 5210). Time series data on the ac conductivity at 2 kHz were measured by using the digital lock-in amplifier and an analog memory recorder (YOKOGAWA, AR1100).

The conductivity was measured at the sensitivity within $\pm 10^{-11}\,\Omega^{-1}\,cm^{-1}$. All the measurements were at isothermal condition (at temperatures), controlled by the computer within ± 0.1 K in sequential measuring runs. At each temperature, with a sampling time of 50 ms, 5000 data points were collected for the time series data.

Table 1
The dimensions of the samples, $Tm(NO_3)_3 6H_2O$, used for the present measurements, in thickness (cm) and in area (cm^2)

Sample $Tm(NO_3)_3 6H_2O$ c-axis	cm in thickness (± 0.005)	cm^2 in area (± 0.005)
A_1	0.113	0.181
A_2	0.536	0.132
A_3	0.337	0.035
B	0.036	0.233

3. Results and discussion

3.1. Temperature dependence of ac conductivity

Fig. 1 shows the real component $\sigma'(T)$ for complex conductivity σ^* ($\sigma^* = \sigma' + i\sigma''$) along c-axis of $Tm(NO_3)_3 6H_2O$ at 1 kHz in a semilogarithmic scale at temperatures T between 293.15 and 203.15 K in cooling and heating cycles of five measuring runs (1)–(5) for the sample A_3 in Table 1.

As seen from Fig. 1, the values of $\sigma'(T)$ in cooling and heating cycles of run (1) show appreciable temperature variation of $\sigma'(T)$ with thermal hysteresis in the region between 283.15 and 203.15 K. The temperature variation of $\sigma'(T)$ as found in the following runs (2) and (3) was attributed to an existence of meta-stable phase in the crystal. In the subsequent measuring runs (4) and (5), the behaviors of $\sigma'(T)$ were unable to be observed in the temperature range, and corresponded to the disappearance of meta-stable phase.

Detailed behavior of meta-stable phase in other rare-earth nitrate crystals was dependent on the rare-earth ion R^{3+} in $R(NO_3)_3 6H_2O$; non-periodic oscillation of appearance for meta-stable phase in $Sm(NO_3)_3 6H_2O$ [6];

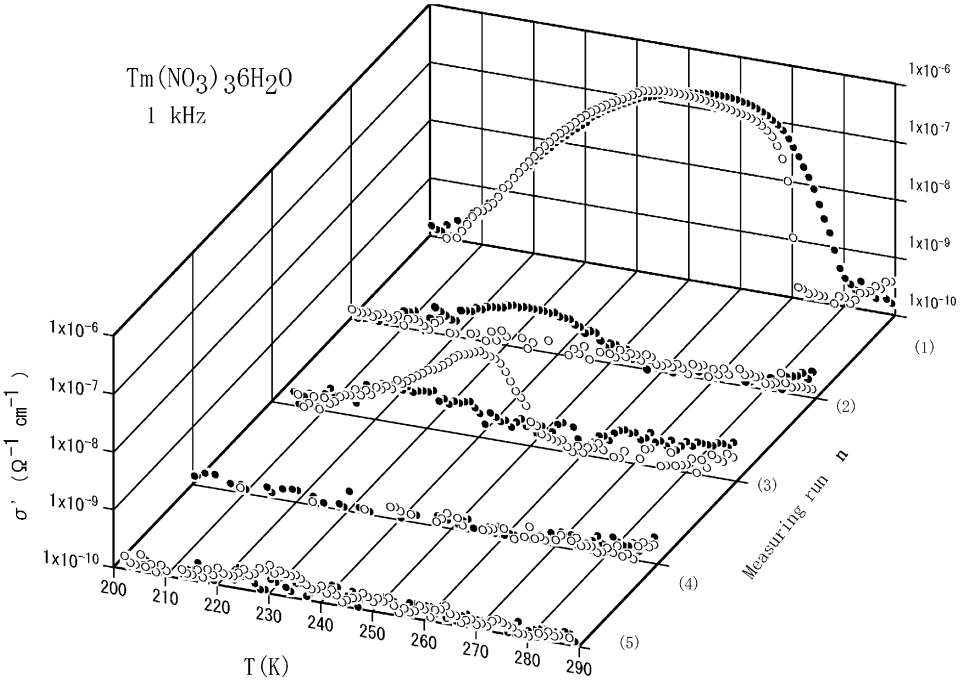

Fig. 1. The real part σ' of the complex conductivity σ^* at 1 kHz along c-axis of $Tm(NO_3)_3 6H_2O$ crystal at temperatures T between 293.15 and 203.15 K in cooling (●) and heating (○) of five measuring runs.

rapid disappearance of the phase in $La(NO_3)_3 6H_2O$ [10], $Nd(NO_3)_3 6H_2O$ [11], $Tb(NO_3)_3 6H_2O$ [12] and $Er(NO_3)_3 6H_2O$ [13]; asymptotic disappearance of the phase in $Gd(NO_3)_3 6H_2O$ [14]; complex behavior appearance of the phase in $Eu(NO_3)_3 6H_2O$ [15] and $Yb(NO_3)_3 6H_2O$ [16].

3.2. Frequency spectra of ac conductivity

Fig. 2 shows the frequency dependence of $\sigma'(v)$ in the logarithmic plane within the range $1\,\mathrm{Hz} \leqslant v \leqslant 10^5\,\mathrm{Hz}$ at several typical temperatures 283.15, 273.15 and 233.15 K in cooling (1) of the first measuring run and at 203.15K in cooling (5) of the fifth run. The values of $\sigma'(v)$ increase with slowly continuous curvature by increasing frequency v at 273.15 and 233.15 K in cooling (1), where temperature variation of σ' was observed in the run. As also seen from Fig. 2, the frequency dependence of $\sigma'(v)$ was represented by the power law $\sigma' \propto v^s$, where v is frequency and s is frequency exponent. The value of the exponent s was derived by calculating the local slope $-\partial \ln \sigma'(v)/-\partial \ln v$ for the spectra of the conductivity. The exponent s in the frequency region $10^4\,\mathrm{Hz} \leqslant v \leqslant 10^5\,\mathrm{Hz}$ is given as a function of temperature T in Fig. 3 for the first and the fifth measuring runs.

As seen in Fig. 3, the value of s decreases and is nearly equal to 0 for meta-stable phase. The value $s \leqslant 1$ has been found in a frequency-dependent conductivity in disordered materials, such as an amorphous semiconductor and glass material [17]. The behavior of $\sigma'(v)$ in meta-stable phase is similar to that of the nearly constant loss in ionic conducting glass [18].

3.3. Dielectric relaxation process

Diagrams of complex conductivity (σ'' against σ') are given in Fig. 4 at several temperatures in cooling (1) and

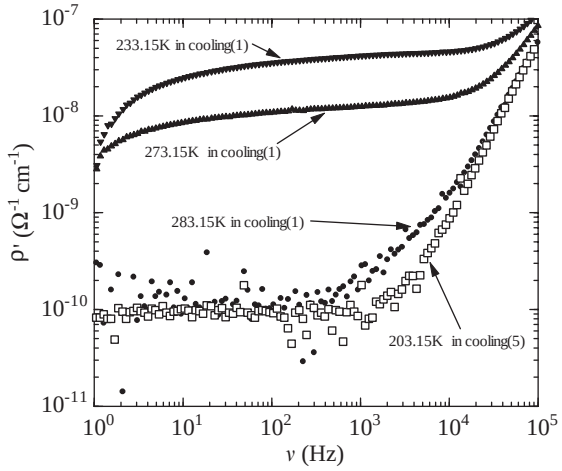

Fig. 2. Frequency dependence of the conductivity σ' along c-axis of $Tm(NO_3)_3 6H_2O$ crystal at several temperatures in the cooling (1) and (5) of the measuring processes.

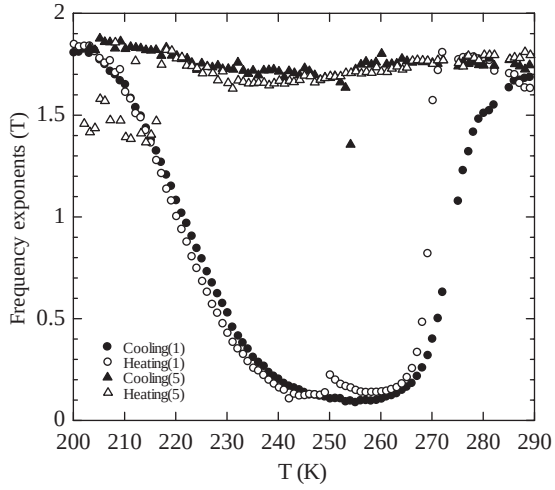

Fig. 3. Frequency exponent $s(T)$ to characterize the power law in the frequency spectra of ac conductivity in the region, 10^4–10^5 Hz, in cooling (1) and (5).

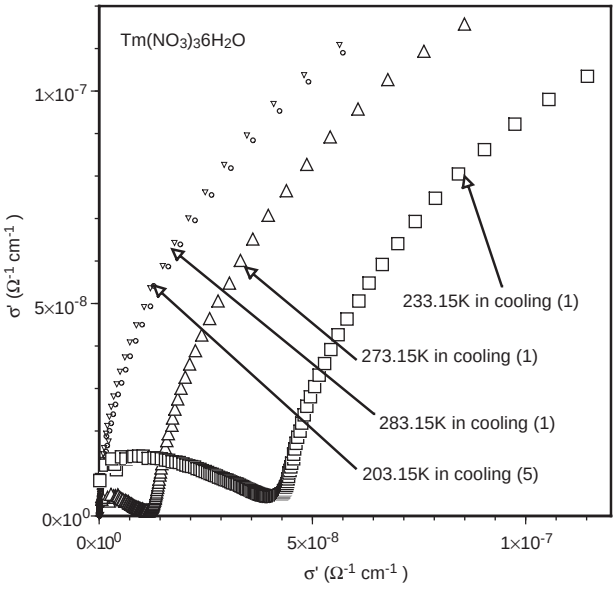

Fig. 4. Representation of the frequency spectra for the ac conductivity on the complex plane of the conductivity at 283.15, 273.15, 233.15 and 203.15 K in cooling (1) and (5).

(5). Larger semicircles are observed in the diagrams at all temperatures in the measuring cycles, and smaller circle at 273.15 and 233.15 K in cooling (1). The double circles were only detectable on the complex plane at temperatures in run (1), for meta-stable phase.

The semicircles in the figure were attributed to a dielectric relaxation process [19]. In Fig. 4, the centers of the circles lie below the σ'-axis. The property of the $\sigma^*(v)$ is classified into a polydispersive relaxation process with a distribution of relaxation time [20]. The complex conductivity $\sigma^*(v)$ with the polydispersive relaxation

process could be expressed by

$$\frac{\sigma^*(\nu)-\sigma_\infty}{\sigma_0-\sigma_\infty}=\frac{1}{1+(i2\pi\nu\tau)^\beta} \quad (1)$$

in which the adjustable parameter β indicates the degree of the distribution of the relaxation time τ. If $\beta=1$ in Eq. (1), the relaxation process is Debye type and the relaxation time is single. The values of β, σ_0 and σ_∞ in Eq. (1) were derived from the numerical data of the frequency spectra for the conductivity in these ranges of temperatures [11].

The larger circle is assigned to the frequency variation of $\sigma^*(\nu)$ in the higher-frequency range $10^4\text{Hz}\leqslant\nu\leqslant 10^5\text{Hz}$, and the smaller one to that in the lower-frequency range $10^4\,\text{Hz}\leqslant\nu\leqslant 10^2\,\text{Hz}$. Figs. 5 and 6 show temperature dependence of the parameters β and the relaxation times τ derived in both the lower- and the higher-frequency regions, respectively, at temperatures from 293.15 to 203.15 K in cooling and heating cycles of runs (1) and (5).

In meta-stable phase, there was polydispersive relaxation process having both the relaxation time τ of 10^{-2}–10^{-3} s and $\beta<1$ with thermal hysteresis. In both stable and meta-stable phases, on the other hand, there was mono-dispersive relaxation process with τ of 10^{-7}–10^{-8} s and $\beta\sim1.0$.

The relaxation times $\tau(T)$ of 10^{-2}–10^{-3} and 10^{-7}–10^{-8} s are longer in comparison with those of 10^{-10}–10^{-11} s in the dielectric relaxation process for the ferroelectric crystals having the dynamic response of molecular dipoles [21]. The relaxation processes are related to the characteristic structure of the rare-earth nitrate [5,19].

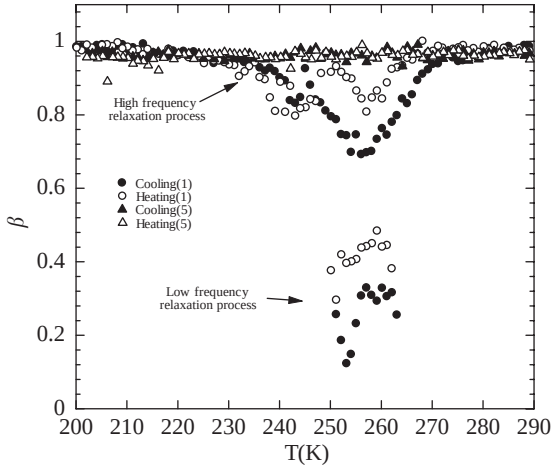

Fig. 5. The parameters $\beta(T)$ to characterize the degree in distribution of relaxation time for both the relaxation processes given in the frequency spectra for the ac conductivity in both frequency regions, 1–10^2 and 10^4–10^5 Hz, respectively, at temperatures $203.15\,\text{K}\leqslant T\leqslant 293.15\,\text{K}$ in cooling and heating cycles of measuring runs (1) and (5).

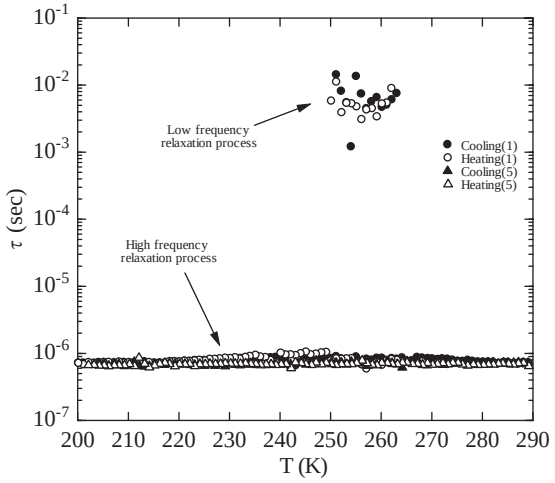

Fig. 6. The relaxation times $\tau(T)$ for both the lower- and the higher-frequency relaxation processes given for the frequency spectra of the ac conductivity in both frequency regions, 1–10^2 and 10^4–10^5 Hz, respectively, at temperatures $203.15\,\text{K}\leqslant T\leqslant 293.15\,\text{K}$ in cooling and heating cycles of measuring runs (1) and (5).

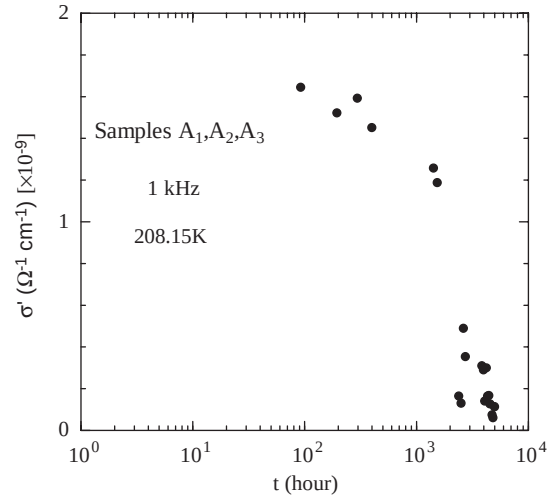

Fig. 7. The dependence of the real part σ' of the complex conductivity at 1 kHz on the ageing periods at 208.15 K, where the aging period is defined as the time elapsed after the mother crystal was grown.

3.4. Aging effect

In the subsequent measuring runs, however, the similar behaviors were unable to be observed in the temperature range. In the temperature region, $T<208.15$ K, σ' are almost independent of the temperature in the subsequent courses of the measuring runs. The behaviors of σ' at 208.15 K are normal in the subsequent measuring runs; in Fig. 7 σ' are plotted as a function of aging periods. The time given in this figure represents the elapse of time measured from the time when the virgin crystal was taken out from the solution of the thulium nitrate. As found in Fig. 7, the value of σ'

shows stepwise variation at the period of about 2×10^3 h.

In Fig. 8, the values of the frequency exponent s at 208.15 K are plotted as a function of the ageing period. The value of s shows independent on the ageing period in the figure.

In Figs. 9 and 10, the values of β and τ in the stable relaxation processes at 208.15 K are plotted as a function of the ageing periods from the crystal growth till the measuring run. From Fig. 9, the values of β approach to 1 as the ageing periods increase. The variation of τ in the ageing process is seen in Fig. 10. The

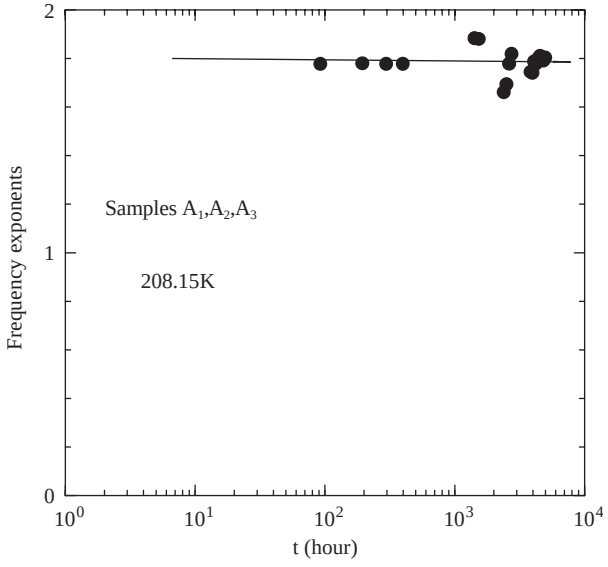

Fig. 8. The frequency exponent s for the power law of the frequency spectra of the ac conductivity at 208.15 K as a function of the ageing periods t (hours) after the crystal growth.

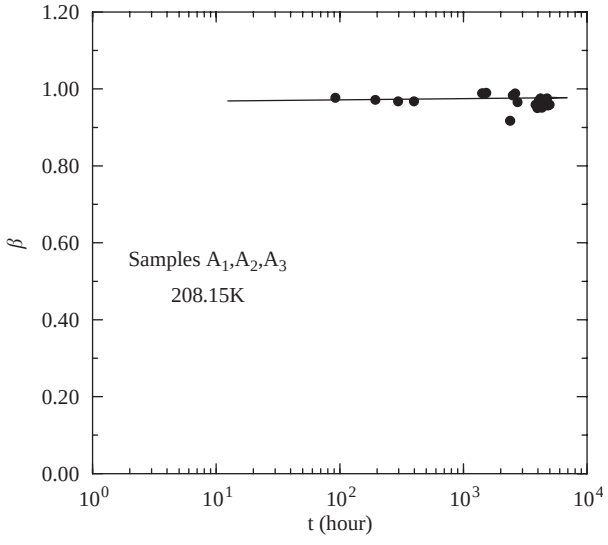

Fig. 9. The parameter β at 208.15 K as a function of the ageing periods t (hours) after the crystal growth.

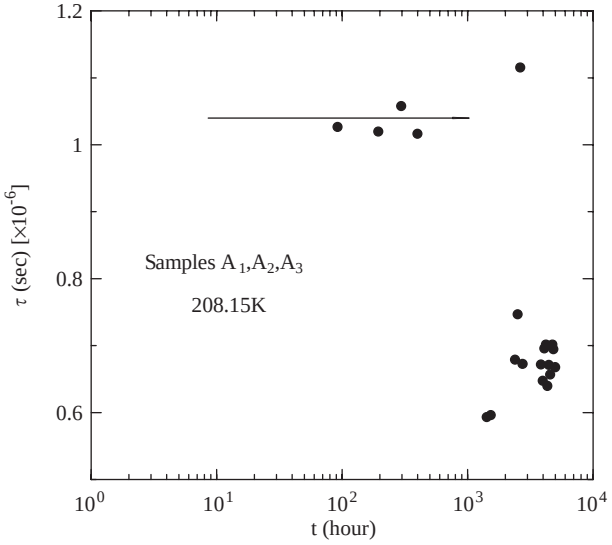

Fig. 10. The relaxation time τ at 208.15 K as a function of the ageing periods t (hours) after the crystal growth.

relaxation time τ is a parameter to characterize the dynamical property of the fluctuation in the materials [20], and hence the fact would be attributed to the variation in the mechanism of the fluctuation in the ageing process.

The aging phenomenon from the meta-stable virgin crystal state to the stable state was classified to a slow structural relaxation process [22]. The phenomenon was caused by the memory effect, and attributed to a non-equilibrium behavior as known in glassy systems [23]. Examples of the behavior have been found in lanthanum nitrate and terbium nitrate crystals [10,12]. Consequently, the aging effect observed is related to non-equilibrium structure of these crystals.

3.5. Time series of ac conductivity

Fig. 11 shows the time-dependent fluctuation $\Delta\sigma'(t)$ in the real part σ' of the complex conductivity σ^* along the c-axis of the $Tm(NO_3)_3 6H_2O$ crystal at several temperatures in cooling cycles, where $\Delta\sigma'$ is given as $\Delta\sigma' = \sigma' - \langle\sigma'\rangle$. The value of $\langle\sigma'\rangle$ was average in 5000 data points of σ' at the temperature. The set of the data $\Delta\sigma'$ is represented by $\{\Delta\sigma'\}$. As found in Fig. 11, non-periodic unstable oscillations (bursts) were found in the time series data $\{\Delta\sigma'\}$ at 223.15 and 203.15 K in cooling, respectively.

The probability distributions of the fluctuation $\{\Delta\sigma'\}$ in the conductivity show continuous line shapes. The power spectrum densities were derived from the time series data $\{\Delta\sigma'\}$. Fig. 12 gives a function of the statistical frequency for the power spectral density at several temperatures in the cooling cycle.

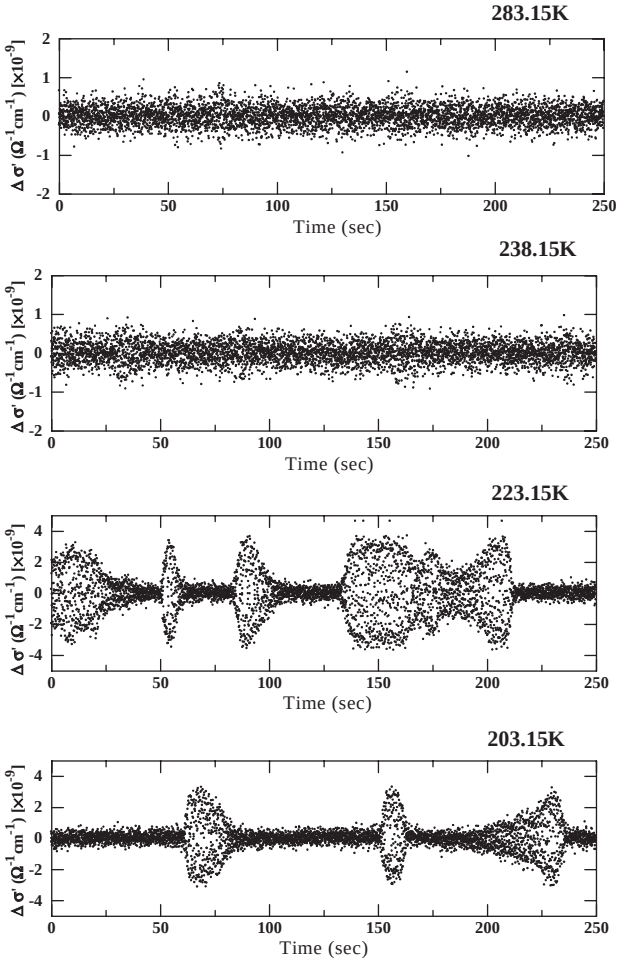

Fig. 11. Time series behaviors of the fluctuation $\Delta\sigma'$ for the real part σ' of the complex conductivity σ^* at 2 kHz for several temperatures in cooling cycle with a sampling time 50 ms along c-axis of $Tm(NO_3)_3 6H_2O$ crystal.

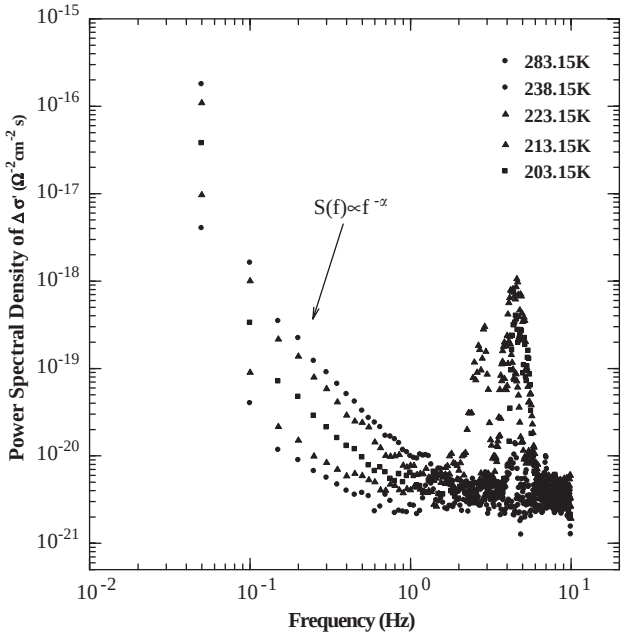

Fig. 12. Log–log plots of the power spectral density $S(f)$ for statistical frequency f (Hz) derived from the time series of the fluctuation $\Delta\sigma'$.

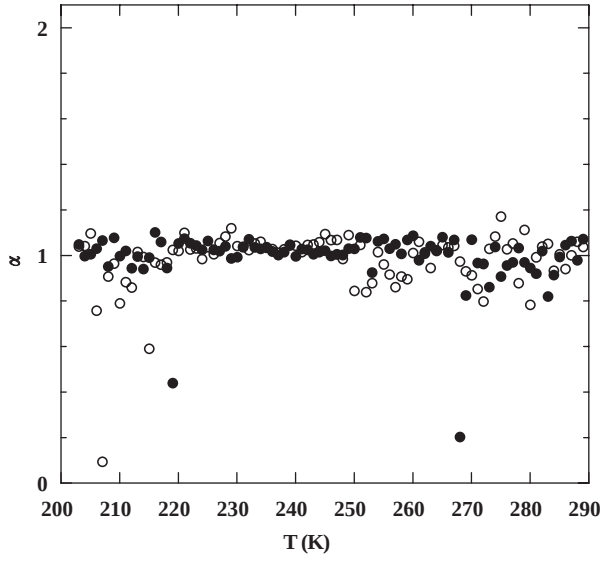

Fig. 13. Temperature dependence of exponent α ($0.1\,\text{Hz} \leqslant f \leqslant 0.5\,\text{Hz}$) in the power law $1/f^{\alpha}$ in the power spectral density of the fluctuation $\Delta\sigma'$ in cooling (●) and heating (○).

In Fig. 12, the power spectral densities of the fluctuation $\{\Delta\sigma'\}$ at temperatures show random broad peaks in the statistical frequency region from 1 to 10 Hz, and continuous line shape below 1 Hz. In the frequency region 0.1–1 Hz, the continuous part of the power spectra is proportional to $1/f^{\alpha}$, where f is the statistical frequency given in the power spectra and α is exponent of the power law. The values of α were derived by calculating the local slopes of the power spectra in the frequency region at temperatures $203.15\,\text{K} \leqslant T \leqslant 293.15\,\text{K}$. The temperature dependence of the exponent α is given in Fig. 13 for cooling and heating cycles of the measuring run. In Fig. 13, the exponent of α is approximately $\alpha \fallingdotseq 1$ in the temperature region and the power spectra assigned to $1/f$ noise [24].

3.6. Non-linear dynamical property

The noticeable non-periodic unstable oscillation (the burst) was the time series data $\{\Delta\sigma'\}$ at 223.15 K as given in Fig. 11. Non-linear dynamical structure of the data was analyzed in detail. As seen in Fig. 14, the time series data of $\Delta\sigma'$ were characterized by two different time domains (a) and (b); the time series data points between 135 and 155 s (500 data points) are assigned to unstable fluctuation time domain (a); the data points between 225 and 250 s (500 data points) to stable non-periodic time domain (b).

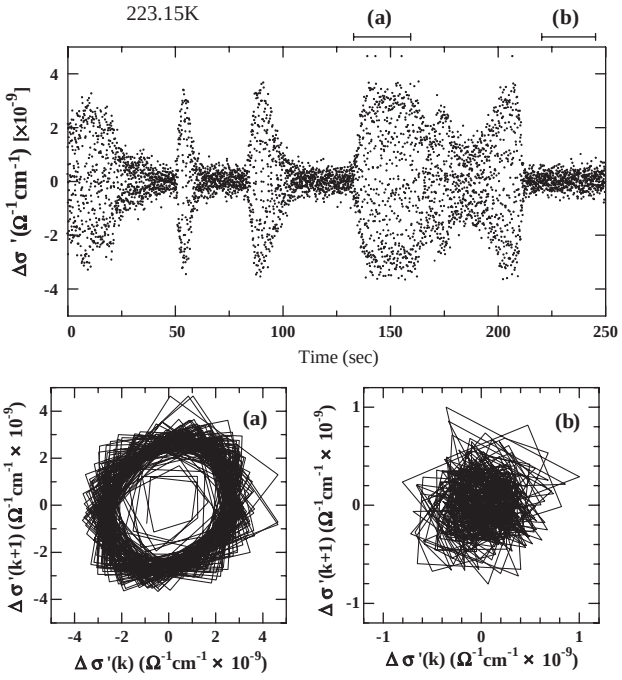

Fig. 14. One-dimensional return maps constructed from the time series of the fluctuation $\Delta\sigma'$ at 223.15 K in cooling in the non-periodic unstable fluctuated time domain (a) and the stable time domain (b), respectively.

Fig. 14 gives one-dimensional return maps for the phase portrait, $\Delta\sigma'(k+1)$ vs. $\Delta\sigma'(k)$, constructed in two different time domains (a) and (b), respectively. The $\Delta\sigma'(k)$ is the value of $\Delta\sigma'$ at an index k ordered from the starting point in the time series data $\{\Delta\sigma'\}$. The return map in the time domain (b) shows a circle pattern overlapped as seen from Fig. 14(b), on the other hand, apparent limit cycles can be found in the time domain (a) from Fig. 14(a).

The obvious limit cycle was observable in the measurement of time series of the electric properties of $Tb(NO_3)_3 6H_2O$ [8], but not in the light rare-earth nitrates, Nd [25], Sm [7] and Eu [26]. The limit cycle has been found in the non-linear and non-equilibrium systems such as Rayleigh–Bernard convection [2], Belousov–Zhabotinski reaction [27] and laser oscillation [28].

The non-linear dynamical property of the system was specified by a fractal dimension derived from N data point of the time series by using the simple procedure of Grassberger and Procaccia [7,29]. For a arbitrary embedding dimension n, the σ'_i and σ'_j are pseudo-vectors defined by

$$\sigma'_i = \{\sigma'(t+\mathrm{i}\tau_N),\ \sigma'(t+(\mathrm{i}+1)\tau_N),\ \ldots,\ \times\sigma'(t+(\mathrm{i}+n-1)\tau_N)\}, \quad (2)$$

where the value of τ_N is a fixed time increment between successive measurements. In the present measurement, τ_N is corresponded to the sampling time, 50 ms. Spatial correlation of the attractor embedded in a phase space

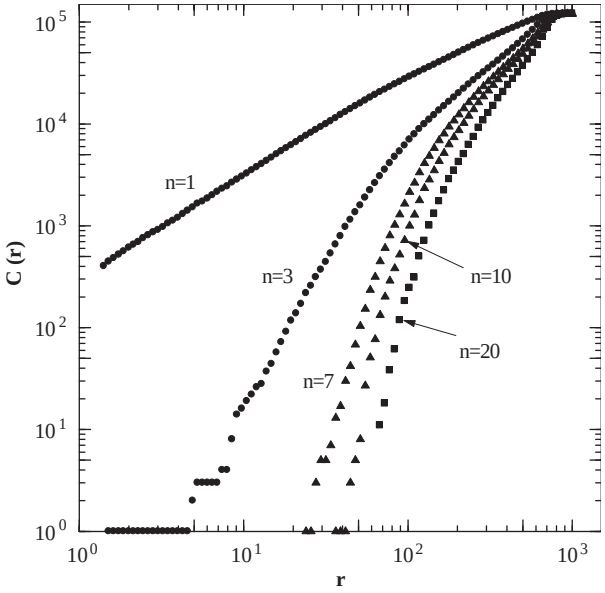

Fig. 15. Log–log plots of the correlation integral $C(r)$ vs. r for increasing values of the artificial phase-space embedding dimension $n = 1\cdots20$ derived from the time series of $\Delta\sigma'$ at 223.15 K.

of n-dimensions is defined by

$$C(r) = \frac{1}{N^2}\sum_{i,j=1}^{N}\theta(r-|\sigma'_i-\sigma'_j|), \quad (3)$$

where $\theta(x)=0$ if $x<0$ and $\theta(x)=1$ if $x>0$. The correlation integral, $C(r)$, of the attractor embedded in the phase space of n-dimensions counts the number of pairs whose distance $|\sigma'_i-\sigma'_j|$ is smaller than a given r.

The values of the correlation integral $C(r)$ were calculated for the time series data $\{\Delta\sigma'\}$ at temperatures by using the supercomputer (SR8000, Hitachi) of Hokkaido University. The correlation integrals $C(r)$ at 223.15 K in cooling cycle are shown in Fig. 15 for the embedding dimension $n = 1\cdots20$. The correlation integral $C(r)$ behaves as power of r for small r: $C(r)\propto r^d$, where d is a correlation exponent. The values of the correlation exponent d at each embedding dimension n were derived from the slope of $\ln C(r)$ vs. $\ln r$.

Fig. 16 shows the dependence of the correlation exponent d on the embedding dimension n, given as $d(n)$, at the temperatures in heating cycle, respectively. The straight line $d=n$ is assigned to the case of the random noise. As seen from Fig. 16, the values of the correlation exponent d at 223.15 K in cooling cycle reache asymptotic ones as the value of the embedding dimension n increases.

4. Summary

The phenomenological structure of the meta-stability for the rare-earth nitrate crystals was studied by

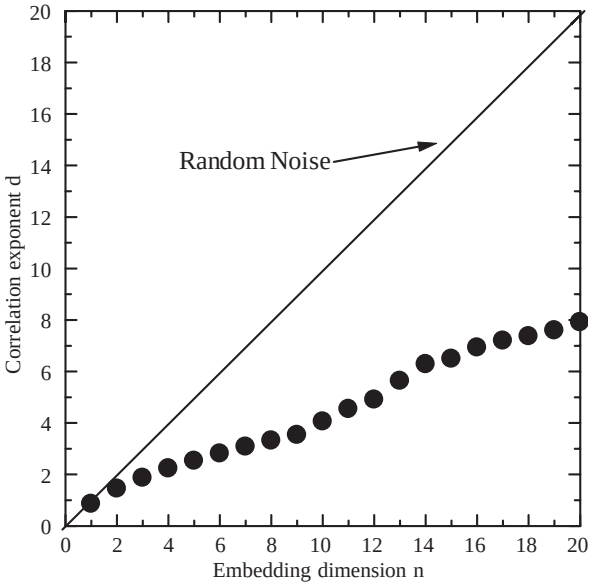

Fig. 16. Correlation exponent d vs. the dimension n of the embedding space derived from the time series of $\Delta\sigma'$ at 223.15 K.

measuring the electric properties of $Tm(NO_3)_36H_2O$ crystal. In meta-stable phase, the frequency response of ac conductivity was expressed by power law having the value of the exponent s, $0 \leqslant s \leqslant 1$ as seen in the disordered system. Moreover, the meta-stable slow dispersive relaxation process emerged. The ageing effect on the value of the conductivity and the relaxation time was found.

The burst (non-periodic-instability) was observed in the time series data of the conductivity. The limit cycle was seen in the return map constructed from the time series data. The dependence of the correlation exponent on the embedding dimension was saturated, and hence the possibility of the chaotic character in the physical properties of the crystal with the meta-stability.

These results in $Tm(NO_3)_36H_2O$ specified the ultimate earmark for the meta-stability in the rare-earth nitrate crystals.

The meta-stability in the rare-earth nitrate crystals depends on rare-earth element [9]. The origin of the meta-stability in the rare-earth nitrate crystal could be attributed to non-linear dynamical microscopic characteristics of the rare-earth element. To deepen understanding of the meta-stability, it is necessary to measure the physical properties of the crystal in ultra low temperature region where the quantum mechanical property is dominant.

References

[1] M. Giordano, D. Leporini, M.P. Tosi (Eds.), Non-Equilibrium Phenomena in Supercooled Fluids, Glasses and Amorphous Materials, World Scientific, Singapore, 1996, pp. 61–98, 167–204.
[2] S.K. Scott, Chemical Chaos, Oxford University Press, New York, 1991, p. 125, 1950.
[3] A. Libchaber, J. Maurer, in: T. Riste (Ed.), A Rayleigh Benard Experiment, Helium in Small Box, Non-linear Phenomena at Phase Transitions and Instabilities, Plenum Press, New York, 1981, p. 259.
[4] J. Cai, Y. Kato, A. Ogawa, Y. Harada, M. Chiba, T. Hirata, J. Phys. Soc. Japan 71 (2002) 3087–3091.
[5] R. Kawashima, M. Sasaki, S. Satoh, H. Isoda, Y. Kino, Y. Shiozaki, J. Phys. Soc. Japan 69 (2000) 3297–3303.
[6] R. Kawashima, Y. Matsuda, J. Phys. Soc. Japan 59 (1990) 3727–3731.
[7] R. Kawashima, S. Nishimura, H. Isoda, Physica B 183 (1993) 135–144.
[8] R. Kawashima, R. Hattada, H. Isoda, J. Phys. Soc. Japan 68 (1999) 1143–1147.
[9] R. Kawashima, J. Fukui, K. Haruki, H. Isoda, J. Phys. Soc. Japan 72 (2003) 2477–2481.
[10] R. Kawashima, T. Saitoh, H. Isoda, J. Phys. Soc. Japan 62 (1993) 4529–4530.
[11] R. Kawashima, M. Hattori, H. Isoda, J. Phys. Chem. Solids 55 (1994) 1331–1335.
[12] R. Kawashima, S. Nasukawa, H. Isoda, J. Phys. Soc. Japan 64 (1995) 1439–1440.
[13] R. Kawashima, J. Phys. Soc. Japan 60 (1991) 342–343.
[14] R. Kawashima, H. Isoda, J. Phys. Soc. Japan 59 (1990) 3408–3409.
[15] R. Kawashima, T. Sasaki, H. Isoda, J. Phys. Soc. Japan 63 (1994) 2008–2009.
[16] R. Kawashima, R. Takahashi, H. Isoda, J. Solid State Chem. 121 (1996) 74–78.
[17] S.R. Elliott, Adv. Phys. 36 (1987) 135–217.
[18] K.L. Ngai, C. Leo'n, Phys. Rev. B 66 (2002) 064308-1 (11 pages).
[19] R. Kawashima, H. Takahashi, H. Isoda, J. Solid State Chem. 144 (1999) 354–360.
[20] V.V. Daniel, Dielectric Relaxation, Academic Press, London, 1967, p. 97.
[21] M.E. Lines, A.M. Glass, Ferroelectrics and Related Materials, Oxford, London, 1977, pp. 293–321.
[22] C.C. Angell, et al., in: K. Kawasaki, et al. (Eds.), Slow Dynamics in Condensed Matter, AIP, NY, 1991, pp. 3–19.
[23] S. Franz, et al., Phys. Rev. Lett. 81 (1998) 1758–1761.
[24] P. Dutta, P.M. Horn, Rev. Mod. Phys. 53 (1981) 497–516.
[25] R. Kawashima, T. Fukase, H. Isoda, J. Phys. Chem Solids 57 (1996) 539–545.
[26] R. Kawashima, M. Kawasaki, H. Isoda, Chaos, Solitons Fractal 7 (1996) 1863–1869.
[27] Y. Pomeau, J.C. Roux, A. Rossi, S. Bachelart, C. Vidal, Le J. Phys. Lett. 42 (1981) L271–L273.
[28] F.T. Arecchi, R. Meucci, G. Puccioni, J. Tredicce, Phys. Rev. Lett. 49 (1982) 1217–1220.
[29] P. Grassberger, I. Procaccia, Physica D 9 (1983) 189–208.